Conf-920311--18

ANL/CP--74880

DE92 016183

DYNAMIC MODELING OF PLASMA-VAPOR INTERACTIONS DURING PLASMA DISRUPTIONS

by

Ahmed Hassanein and David A. Ehst

Argonne National Laboratory
Fusion Power Program
9700 South Cass Avenue
Argonne, IL 60439 USA

May 1992

* Work supported by the Office of Fusion Energy, U.S. Department of Energy under Contract Number W-31-109-Eng-38.

Presented at the 10th International Conference on Plasma Surface Interactions in Controlled Fusion Devices, Monterey, California, March 30 - April 3, 1992. To be published in the Journal of Nuclear Materials.

DYNAMIC MODELING OF PLASMA-VAPOR INTERACTIONS DURING PLASMA DISRUPTIONS

A. Hassanein and D.A. Ehst
Argonne National Laboratory
Argonne, IL 60439 USA

Abstract

Intense deposition of energy in short times on fusion reactor components during a plasma disruption may cause severe surface erosion due to ablation of these components. The exact amount of the eroded material is very important to the reactor design and its lifetime. During the plasma deposition, the vaporized wall material will interact with the incoming plasma particles and may shield the rest of the wall from further damage. The vapor shielding may then prolong the lifetime of these components and increase the reactor duty cycle.

To correctly evaluate the impact of vapor shielding effect a comprehensive model is developed. In this model the dynamic slowing down of the plasma particles, both ions and electrons, with the eroded wall material is established. Different interaction processes between the plasma particles and the ablated material are included. The generated photons radiation source and the transport of this radiation through the vapor to the wall is modeled. Recent experimental data on disruptions is analyzed and compared with model predictions. Vapor shielding may be effective in reducing the overall erosion rate for certain plasma disruption parameters and conditions.

1. Introduction

During a plasma disruption an intense flow of energy is directed outward from the plasma core to the reactor vessel components. As a result a sharp deposition of energy in short times occurs on reactor components such as the first wall and the divertor/limiter. This may cause severe surface erosion due to ablation of these components. The exact amount of erosion from the wall material is very important to the reactor design and its lifetime. During the plasma deposition, the ablated wall material will interact with the incoming plasma particles and may shield the rest of the wall from further damage.

Various investigations have attempted to predict the exact damage to the wall during a plasma disruption but the significance of the plasma-vapor interactions had not yet been fully resolved. See, for example, references 1-7. To correctly evaluate the impact of vapor shielding effect a comprehensive model is being developed. Figure 1 shows an illustration of the different processes encountered during plasma-vapor interaction following a plasma disruption. In the model the plasma energy, which is carried by the escaping ions and electrons, is first deposited on the solid wall structure. Melting and vaporization of the wall material immediately follows. The vapor formed due to erosion in front of the wall expands toward the incoming plasma particles. The plasma particles then deposit part of their energy into the vapor and the rest of their energy is deposited into the condensed phase of the wall behind the vapor. As a result more vapor is produced and consequently more plasma energy is deposited into the vapor. Soon after, the plasma particles will completely stop in the vapor and no plasma particle kinetic energy will be able to penetrate through to the condensed wall material. Instead the plasma kinetic energy will be converted into radiation,

in the range of soft x-rays, which in turn will be transported and absorbed partly by the vapor itself and partly by the condensed wall material. The resulting radiation is assumed emitted isotropically which means that part of the produced x-ray energy is directed toward the original disruption spot and the rest is directed away to much larger wall areas with less severe effects.

Recent experimental data on disruption using both electron beam and ion beam simulations is analyzed and compared with model predictions. There are basic differences found between electron beam and ion beam simulations. Both can yield different erosion thicknesses for the same disruption energy and deposition time. Vapor shielding may be effective in reducing the overall erosion rate for certain disruption parameters and conditions.

2. Plasma-vapor interaction

The plasma particles traveling through matter lose energy primarily due to the processes of ionization and excitation of the electron cloud surrounding the nucleus. At low plasma ions energy, elastic nuclear scattering can also result in an appreciable energy loss. For non-relativistic plasma ions, the general Bethe equation is used to describe the bound electron stopping power and has the form [8].

$$\frac{dE}{dx} = \frac{4\pi N_0 Z^2_{eff} \rho e^4 Z_2}{m_e c^2 \beta^2 A_2} \left[\ln \left(\frac{2 m_e c^2 \beta^2 \gamma^2}{\bar{I}} \right) - \beta^2 - \sum_i c_i / Z_2 \right] \qquad (1)$$

where:

Z_1 = atomic number of the projectile ion

Z_{eff} = effective charge of the projectile ion

N_0	=	Avagadro's number
ρ	=	density of the stopping medium
A_2	=	atomic weight of stopping medium
Z_2	=	atomic number of stopping medium
β	=	(particle velocity)/c
c	=	velocity of light in vacuum
m_e	=	electron rest mass
$\bar{I}$	=	average ionization potential
$\sum c_i/Z_2$	=	sum of the effects of shell corrections on the stopping charge
e	=	electronic charge

For low energy ions, the Bethe theory is not appropriate and instead the Linhard model is used. This model makes use of a Thomas-Fermi description of the electron clouds of the ion and the stopping atom due not only to the excitation and ionization of the stopping atoms, but also to the elastic coulomb collisions of the ion and the nucleus of the stopping atom. The electronic stopping power is given by [9]:

$$\frac{dE}{dx} = C_{LSS} E^{1/2} \qquad (2)$$

where C_{LSS} is a constant that depends on both the incident ion and the target material parameters.

The nuclear stopping due to elastic coulomb collisions between the ion and the target nuclei becomes significant at very low ion energies. An expression for the nuclear stopping is given by [10]:

$$\frac{dE}{dx} = \rho C_n E^{1/2} \exp\left(-45.2 (C_n' \cdot E)^{0.277}\right) \quad (3)$$

where:

$$C_n = \frac{4.14 \times 10^6}{A_1^{1/2}} \left(\frac{A_1}{A_1 + A_2}\right)^{3/2} \left(\frac{Z_1 Z_2}{A_2}\right)^{1/2} (Z_1^{2/3} + Z_2^{2/3})^{-3/4} \quad (4)$$

$$C_n' = \frac{A_2}{(A_1 + A_2)} \frac{1}{Z_1 Z_2} (Z_1^{2/3} + Z_2^{2/3})^{-1/2} \quad (5)$$

The total stopping power for an ion slowing down in the vapor or in the condensed material is given by taking the minimum of Bethe (equation 1) or Linhard (equation 2) electronic stopping power and adding to it the above nuclear stopping power (equation 3).

The slowing down of plasma electrons in both the vapor and in the condensed material can be estimated by the following equation [11].

$$\frac{dE}{dx} = \frac{4\pi N_o Z_2 Z^2 e^4}{m_e c^2 \beta^2} \left[\ln\left((\gamma - 1)\sqrt{\frac{\gamma + 1}{2}} * m_e c^2 / \bar{I}\right) - \beta^2/2\right] \quad (6)$$

As the plasma particles heat and ionize the ablated material, more free plasma

electrons are produces which in turn will contribute to the slowing down process. An expression used for both the plasma electron and ion component contribution to the overall stopping power is given in reference [8].

3. Radiation transport

The continuous deposition of the plasma particles energy in the ablated wall material will ionize and eventually create a hot region in the vapor which radiates away some or all of that deposited energy. The radiation temperature is proportional to the fourth root of the energy density of the radiation field. Absorption and emission of radiation by the vapor is modeled with an average energy exchange term between the two media. The equation of state of the vapor as well as the opacities can greatly affect the radiative heat transfer in the vapor [4]. A comprehensive model for the ionization processes and the resulting radiation kinetics and its transport in the ablated material is currently being developed to accurately account for the amount and the spectra of radiation that reaches the condensed wall material. For the calculation presented in this study, a steady flow of energy is assumed. The deposited plasma particles energy in the ablated material is immediately converted to radiation. The transport and absorption of these soft x-ray radiations are calculated from a tabulated cross-sections library for all candidate wall and divertor materials which are implemented in the A*THERMAL-2 computer code [13].

4. Disruption simulation

One main reason for this study is to model recent disruption simulation experiments using both a plasma gun and an electron beam to deposit the energy on target materials [12]. The plasma gun accelerator used a low energy (<100

eV) hydrogen beam to deposit up to 15 MJ/m^2 in 0.1 ms pulse duration. Another plasma gun experiment used an argon plasma to simulate disruption [15]. The electron beam experiment used a 60 KeV electrons to deposit up to 5 MJ/m^2 in a duration of 0.05 - 0.2 ms range. Results from the plasma gun experiments have shown considerably less erosion, about two orders of magnitude lower, than the theoretical results in which no vapor shielding effect is taken into account. Results from the electron beam simulation have shown less shielding effect compared to the plasma gun experiments. Erosion measurements were performed by means of both weight loss and profilometric techniques.

Preliminary computer calculations using the dynamic plasma-vapor interaction model to simulate the above experiments are described below. Figure 2 shows the predicted tungsten target temperature rise and the total eroded thickness as a result of an electron beam induced disruption. The calculation is done for two different energy densities i.e., 1.5 MJ/m^2 and 4 MJ/m^2 deposited in 0.1 ms. The target surface temperature for the case of 1.5 MJ/m^2 continues to increase in time till the end of the deposition time. This temperature profile is similar to profiles where no vapor shielding effect is included [14]. However, the temperature profile for the 4 MJ/m^2 case shows a different behavior. Shortly after the start of the deposition the surface temperature rise begins to decrease as the ablated thickness of the wall material rises sharply. This indicates that the ablated material absorbs some of the incoming electron beam energy.

Figure 3 shows the electron beam energy and the radiated heat flux that reach the condensed tungsten wall during the disruption simulation. While the initial electron energy that reaches the wall at the start of the disruption is 60 KeV, the final energy to the wall at the end of the disruption is about 45 Kev for the 1.5 MJ/m^2 case, indicating little attenuation in the ablated

material and a very small radiation flux to the surface as shown. For the 4 MJ/m^2, the electrons are completely stopped in the ablated material during the last quarter of the deposition and no particle kinetic energy is then deposited at the wall. Instead a higher radiation flux is deposited at the surface of the target. Figure 4 shows the effect of higher energy depositions on the electron kinetic energy and on the radiated heat flux at the condensed target material. The higher the energy density the more the ablated material. This will cause the electrons to be stopped sooner in the vapor and the mechanism of heating the wall will only be from the radiation heat flux that reaches the surface of the target.

Figure 5 shows a comparison between the recent experimental data using the electron beam deposition on tungsten target and the current theoretical calculations. The agreement is quite good for the available data. At the lower energy density of 1.5 MJ/m^2, the expected vapor shielding effect is minimal and the calculation without the shielding effect produces almost the same amount of erosion. However, at the higher energy density of 4 MJ/m^2 the theoretical calculation without vapor shielding effect is about a factor of 3 higher than with the vapor shielding. It seems that the current model predicts the shielding effect of an electron beam disruption simulation quite reasonably.

The analysis of plasma gun experiments to simulate a disruption is presented below. One experiment (USSR) used a hydrogen plasma beam accelerator with a particle energy of a few tens of an eV to deposit up to 12 MJ/m^2 deposited in 0.1 ms on tungsten target [12]. Figure 6 shows the ion energy and the radiated flux at the target surface as a function of time for both tungsten and graphite targets. Because the initial ion energy is very small compared to that of the electron beam simulations, the ions are stopped

much sooner after the deposition starts. Figure 7 shows both the target surface temperature and the total eroded thickness resulting during the plasma gun deposition. For the same deposited energy and deposition time, a plasma gun simulation produces much less erosion than by an electron beam simulation. Another recent plasma gun experiment located at the University of New Mexico (UNM) used an argon plasma to deposit up to 20 MJ/m^2 in 0.1 ms on a graphite target [15]. A comparison between both the argon plasma gun and the hydrogen plasma gun with the current model calculations is shown in Fig. 8. Also shown is the calculation with no shielding for tungsten. The agreement is fairly good between the dynamic model and the experiments especially for the argon plasma on graphite. For the hydrogen plasma on tungsten, particularly at 12 MJ/m^2, the theoretical prediction may underestimate the experimental data. One reason is the possibility of having some electrons accompanying the hydrogen ions in the plasma gun which are capable of penetrating deeper than ions into the target material and can cause more erosion. Another reason is that the radiation transport model may underestimate the radiated flux at the target surface. However, the agreement is still fairly good considering the uncertainties in the experiment itself.

Both the electron beam and the ion beam simulation experiments have shown significant vapor shielding effect. The erosion rates is about one to two orders of magnitude lower than the calculation without vapor shielding. Further refining of the models used in this calculation is underway. In addition, more experiments with different disruption conditions are required to both verify the models and to accurately predict the effectiveness of vapor shielding.

5. Conclusion

A dynamic interaction model of the incident plasma particles with the ablated wall material during a disruption is developed. In this model the slowing down of the incoming plasma particles in the expanding vapor and the resulting radiation and its transport through the vapor to the wall are included. Preliminary analysis indicates good agreement with both electron beam and plasma gun simulation experiments. Further refining of the models used in the analysis is currently underway. More experiments with different disruption conditions are required to verify the models and to assess the validity of vapor shielding.

References

[1] A.M. Hassanein, G.L. Kulcinski, and W.G. Wolfer, J. Nuclear Materials, 103/104 (1981).

[2] B.J. Merrill and J.L. Jones, J. Nuclear Materials, 111/112 (1982).

[3] A. Sestero and A. Ventura, J. Nuclear Materials, 128/129 (1984).

[4] R.R. Peterson, Radiative Heat Transfer in Self-Shielding Vapor Layer During Tokamak Disruptions, UWFDM-537, 1983.

[5] H. Bolt et al., Fusion Engineering and Design 18 (1991).

[6] J.G. Gilligan and D. Hahn, J. Nuclear Materials, 145-147 (1987).

[7] Y.K. Chen and J.R. Howell, AIChE Symposium Series, 80 (1984).

[8] T.A. Mehlhorn, A Finite Material Temperature Model for Ion Energy Deposition in Ion-Driven ICF Targets, SAND 80-0038.

[9] J. Linhard, M. Scharff, and H.E. Schiott, Kgl. Danske Videnskab. Selskab, Mat. Fys. Medd. 33, No. 14 (1963).

[10] J. Linhard and M. Scharff, Phys. Rev. 124, 128 (1964).

[11] J.D. Jackson, Classical Electrodynamics, John Wiley & Sons, 1975.

[12] V.R. Barabash et al., Fusion Engineering and Design 18 (1991).

[13] A.M. Hassanein, J. Nuclear Materials, 122/123 (1984).

[14] A.M. Hassanein, Response of Materials to Severe Heat Fluxes During Operation in Fusion Reactors, ASME, 88-WA/NE-2.

[15] J.F. Crawford and J.M. Gahl, Ablation Measurements Using A Plasma Disruption Simulator, Presented at the 14th IEEE/NPSS Symposium on Fusion Engineering, San Diego, CA, Oct. 1991.

Figure Captions

Figure 1. Schematic illustration of the different processes encountered during a plasma disruption.

Figure 2. Wall surface temperature and eroded thickness from an electron beam deposition.

Figure 3. Electron energy and the radiated heat flux reaching the wall.

Figure 4. Effect of higher energy densities on the electron energy and on the radiated heat flux at the surface.

Figure 5. Comparison between recent experimental data and current model predictions.

Figure 6. Ion energy and the radiated heat flux at the wall for tungsten and graphite.

Figure 7. Wall surface temperature and eroded thickness of both tungsten and graphite.

Figure 8. Comparison between plasma gun experiments and model predictions.

Dynamics of Plasma-Vapor Interactions

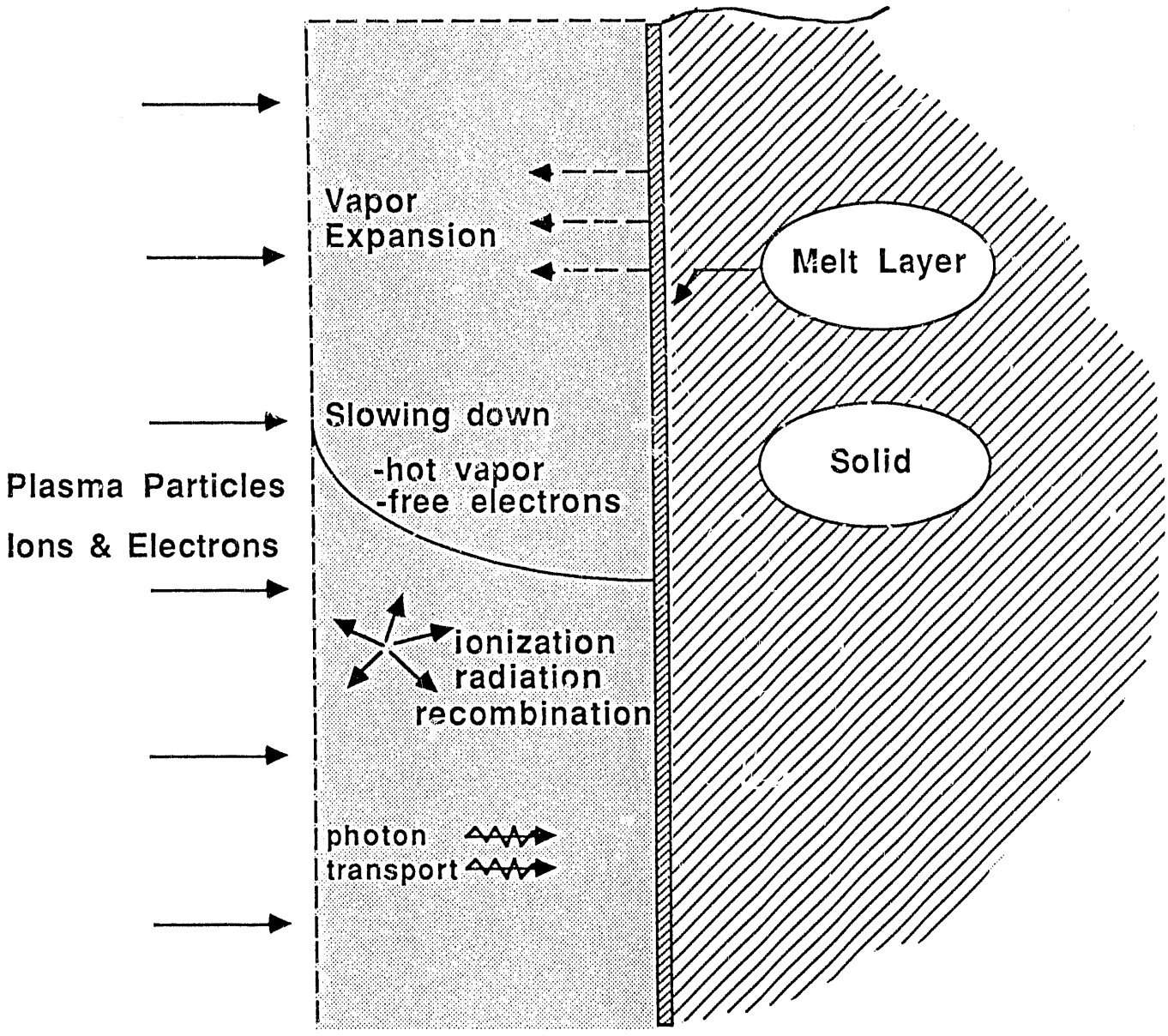

FIGURE 1

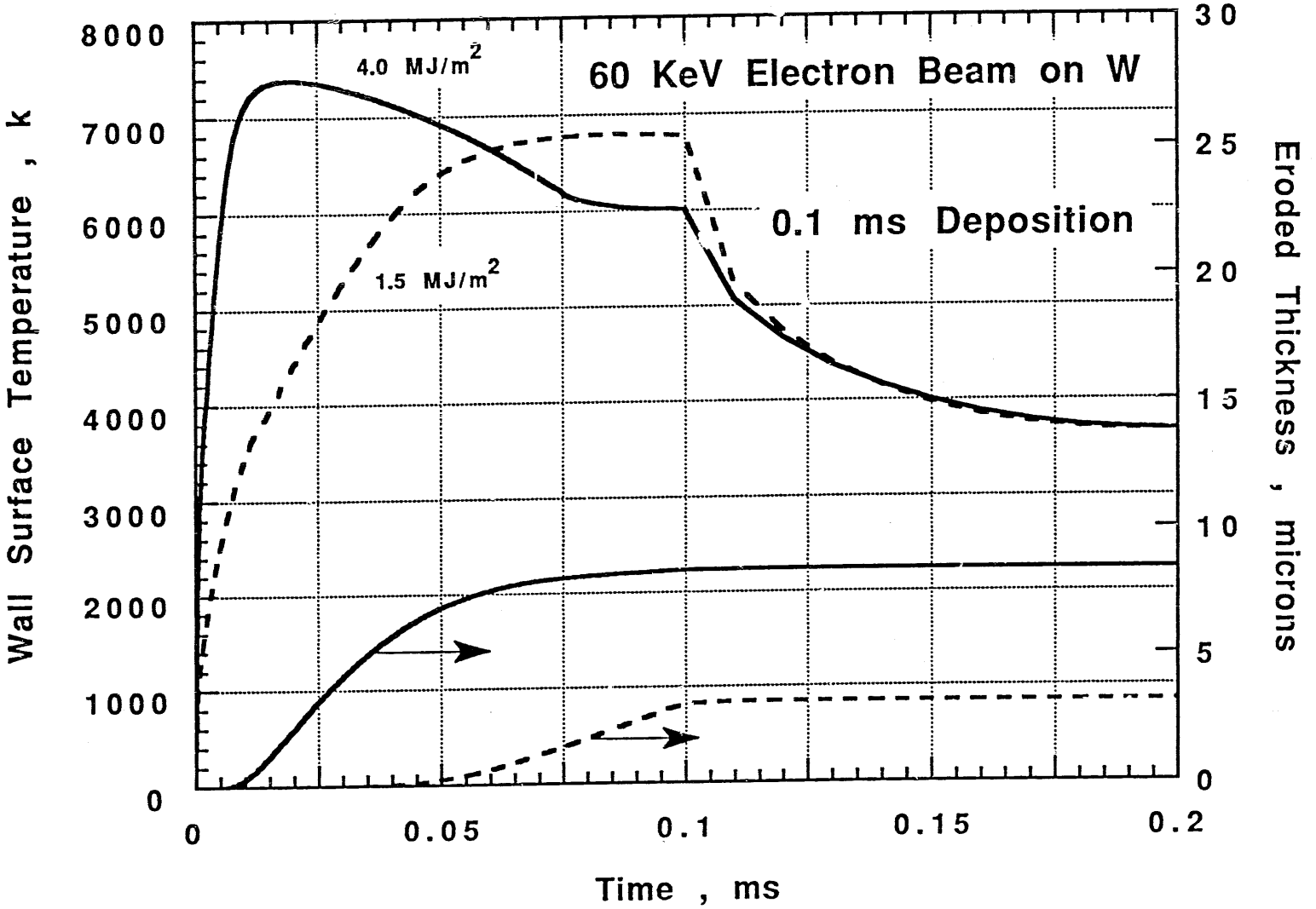
60 KeV Electron Beam on W
0.1 ms Deposition
4.0 MJ/m2
1.5 MJ/m2
Wall Surface Temperature , k
Eroded Thickness , microns
Time , ms
8000
7000
6000
5000
4000
3000
2000
1000
0
30
25
20
15
10
5
0
0
0.05
0.1
0.15
0.2

FIGURE 2

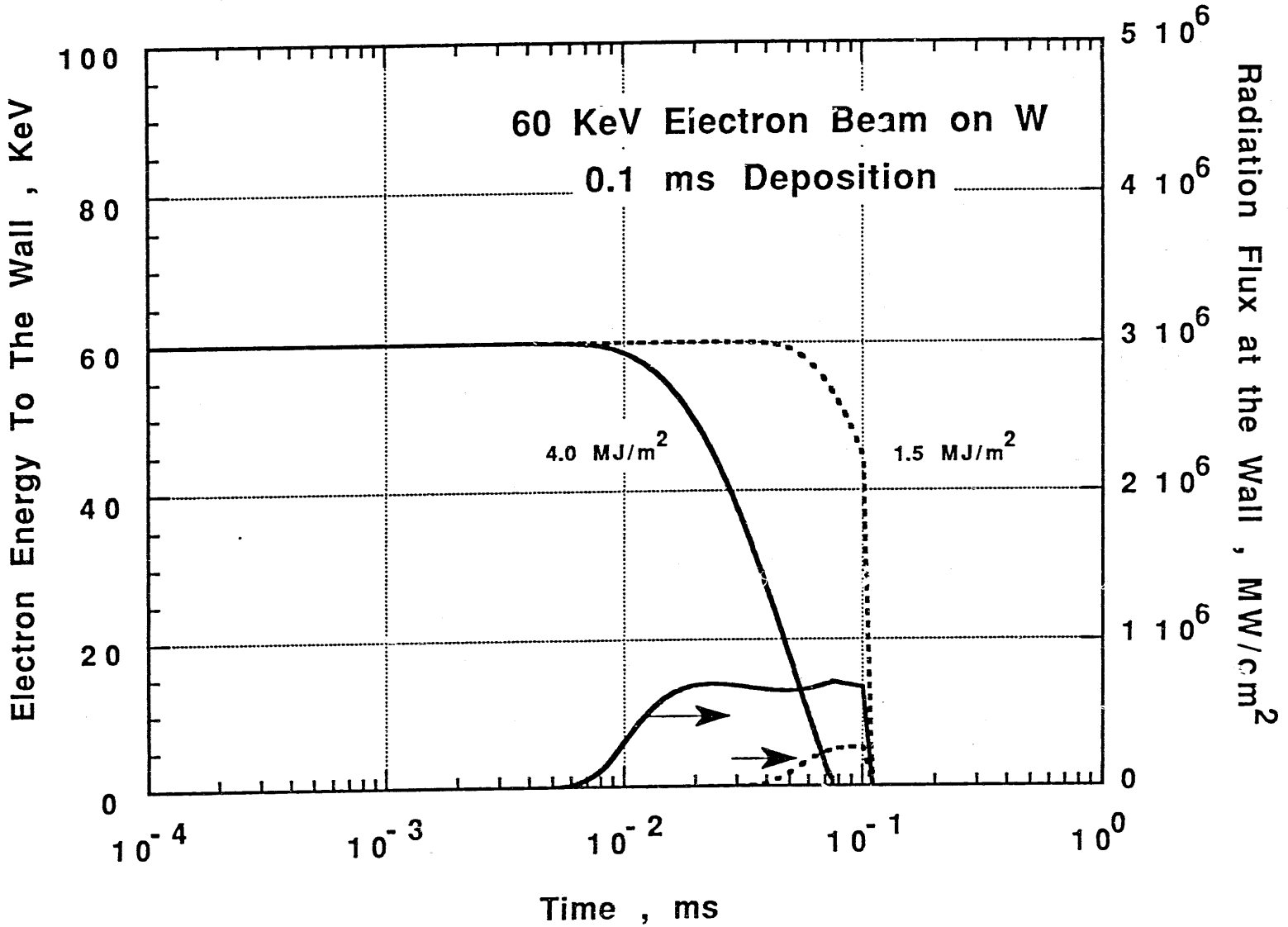
60 KeV Electron Beam on W
0.1 ms Deposition
4.0 MJ/m2
1.5 MJ/m2
Electron Energy To The Wall , KeV
Radiation Flux at the Wall , MW/cm2
Time , ms
100
80
60
40
20
0
5 10^6
4 10^6
3 10^6
2 10^6
1 10^6
0
10^-4
10^-3
10^-2
10^-1
10^0

FIGURE 3

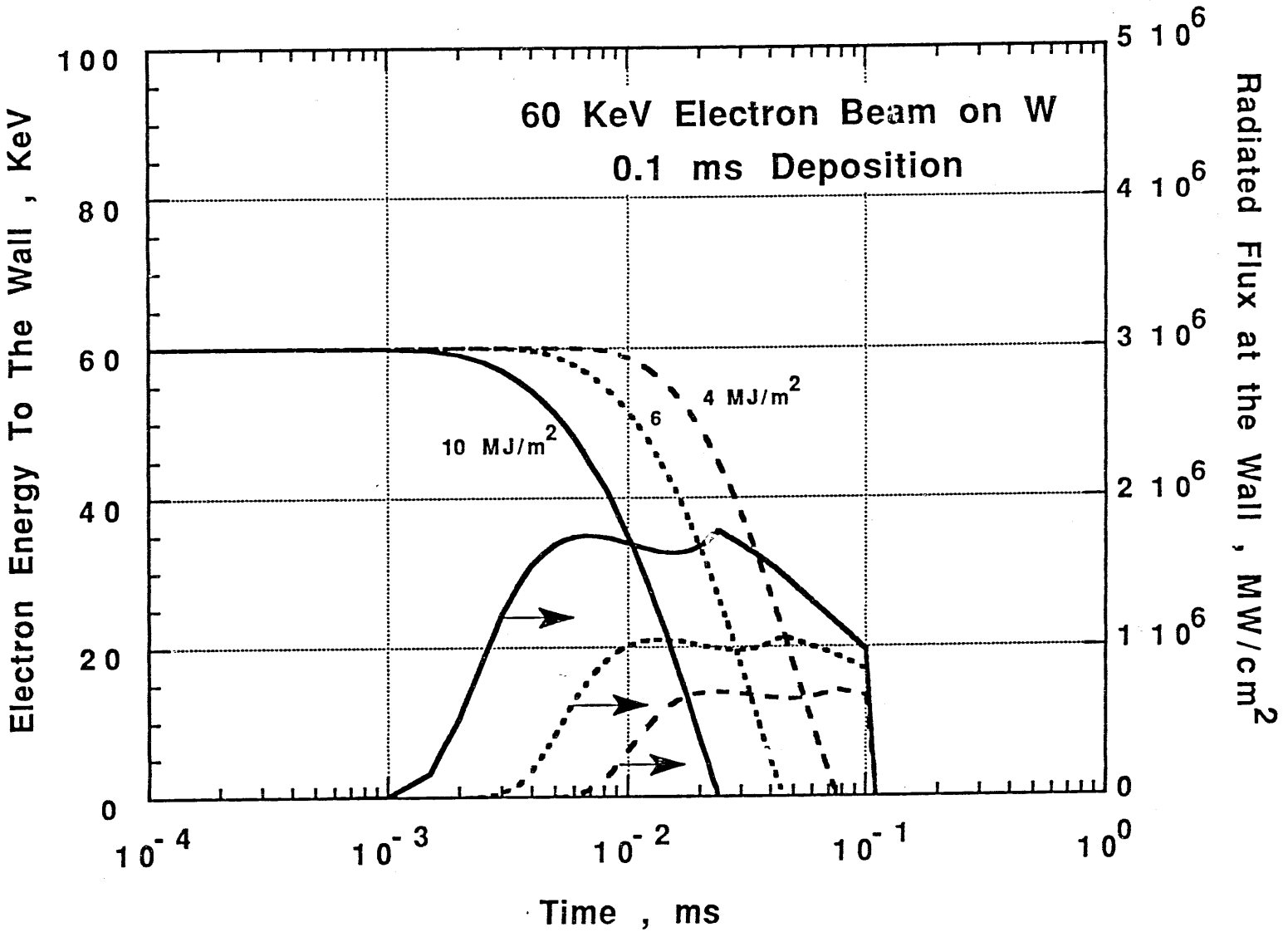
60 KeV Electron Beam on W
0.1 ms Deposition
10 MJ/m2
6
4 MJ/m2
Electron Energy To The Wall , KeV
Radiated Flux at the Wall , MW/cm2
Time , ms
100
80
60
40
20
0
5 10^6
4 10^6
3 10^6
2 10^6
1 10^6
0
10^-4
10^-3
10^-2
10^-1
10^0

FIGURE 4

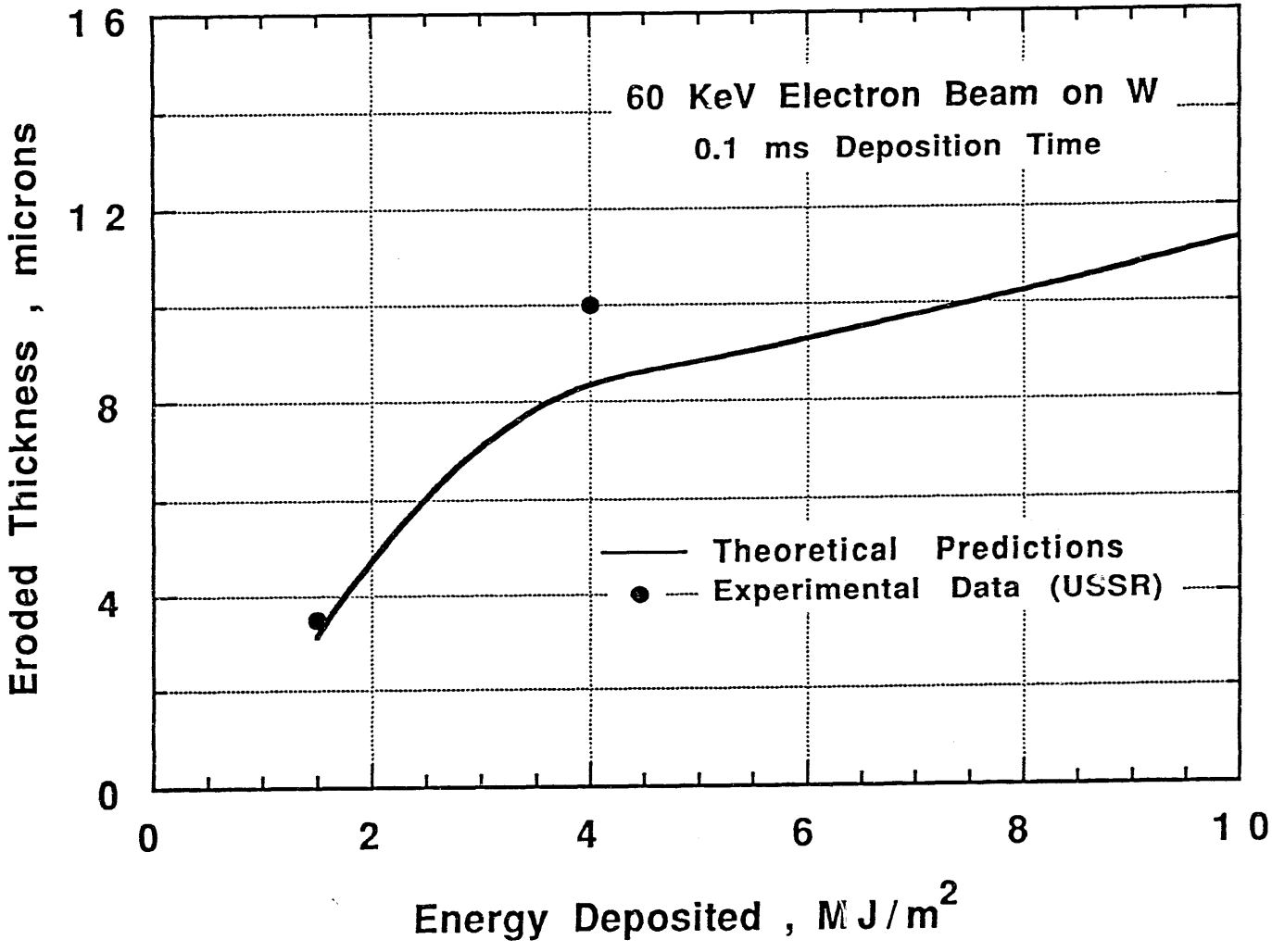
16
12
8
4
0
0
2
4
6
8
10
Eroded Thickness , microns
Energy Deposited , MJ/m2
60 KeV Electron Beam on W
0.1 ms Deposition Time
Theoretical Predictions
Experimental Data (USSR)

FIGURE 5

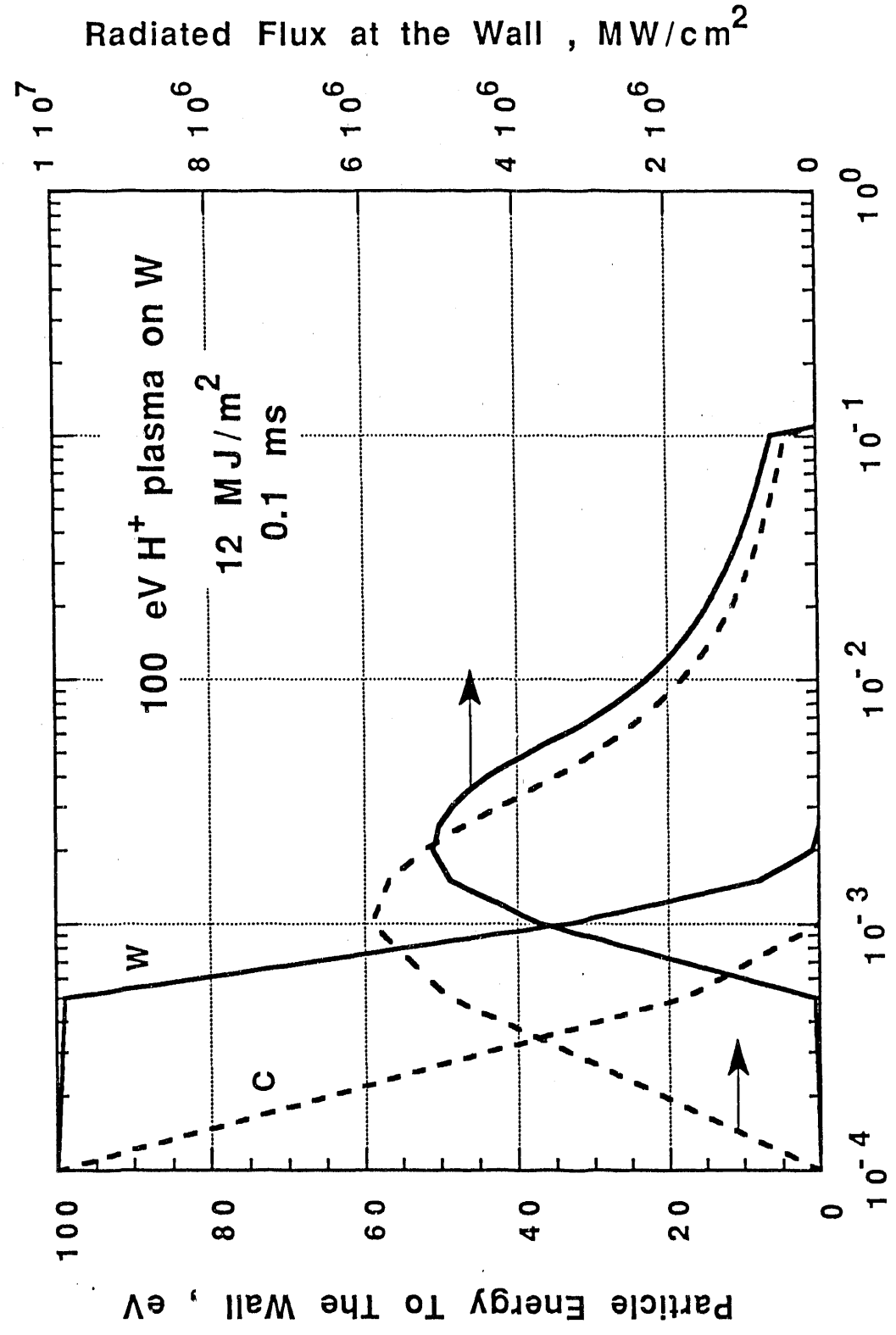
Radiated Flux at the Wall , MW/cm2
1 10 7
8 10 6
6 10 6
4 10 6
2 10 6
0
100 eV H+ plasma on W
12 MJ/m2
0.1 ms
W
C
100
80
60
40
20
0
Particle Energy To The Wall , eV
10 0
10 -1
10 -2
10 -3
10 -4
Time , ms

FIGURE 6

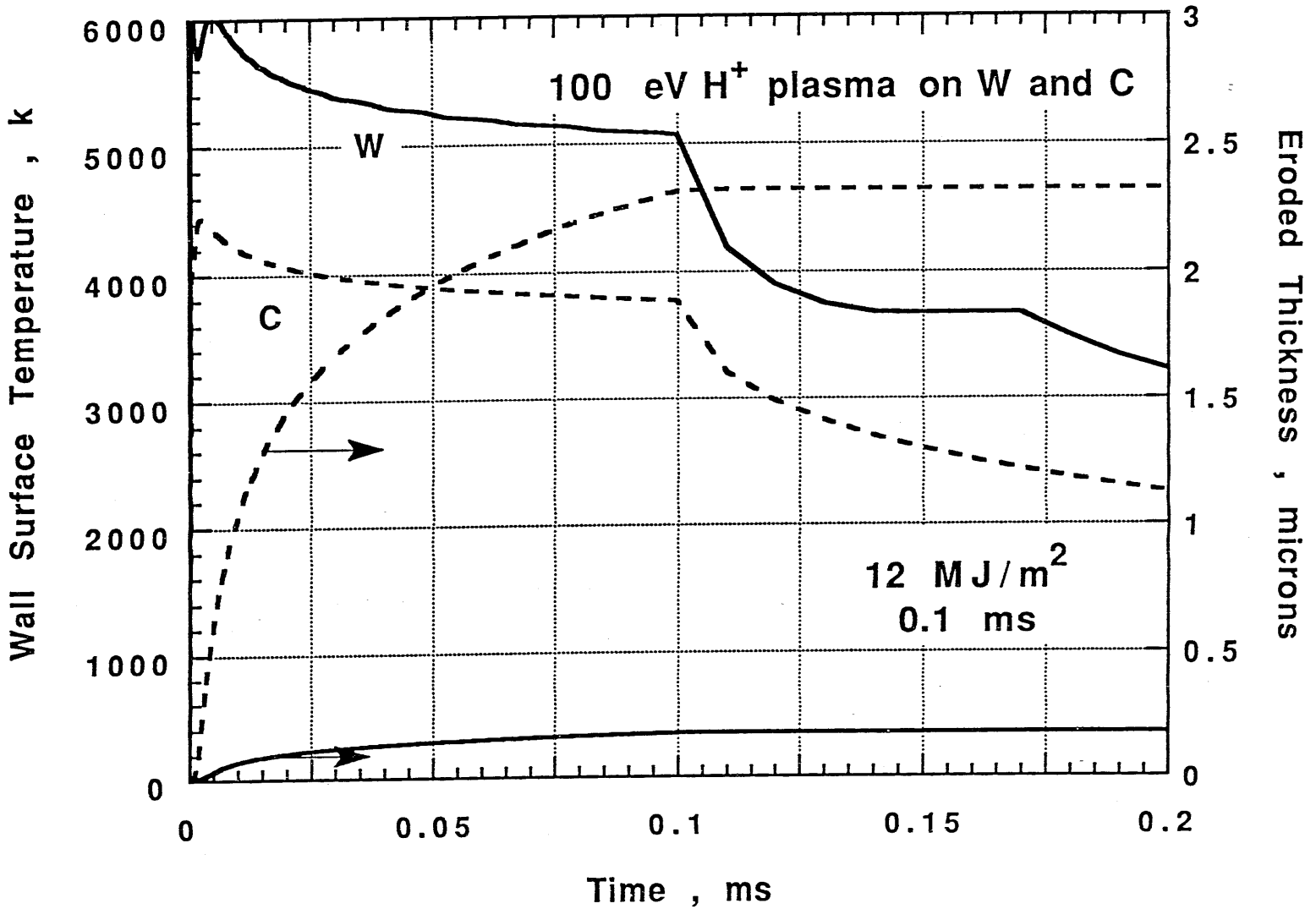
100 eV H+ plasma on W and C
W
C
12 MJ/m2
0.1 ms
Wall Surface Temperature , k
Eroded Thickness , microns
Time , ms
6000
5000
4000
3000
2000
1000
0
3
2.5
2
1.5
1
0.5
0
0.05
0.1
0.15
0.2

FIGURE 7

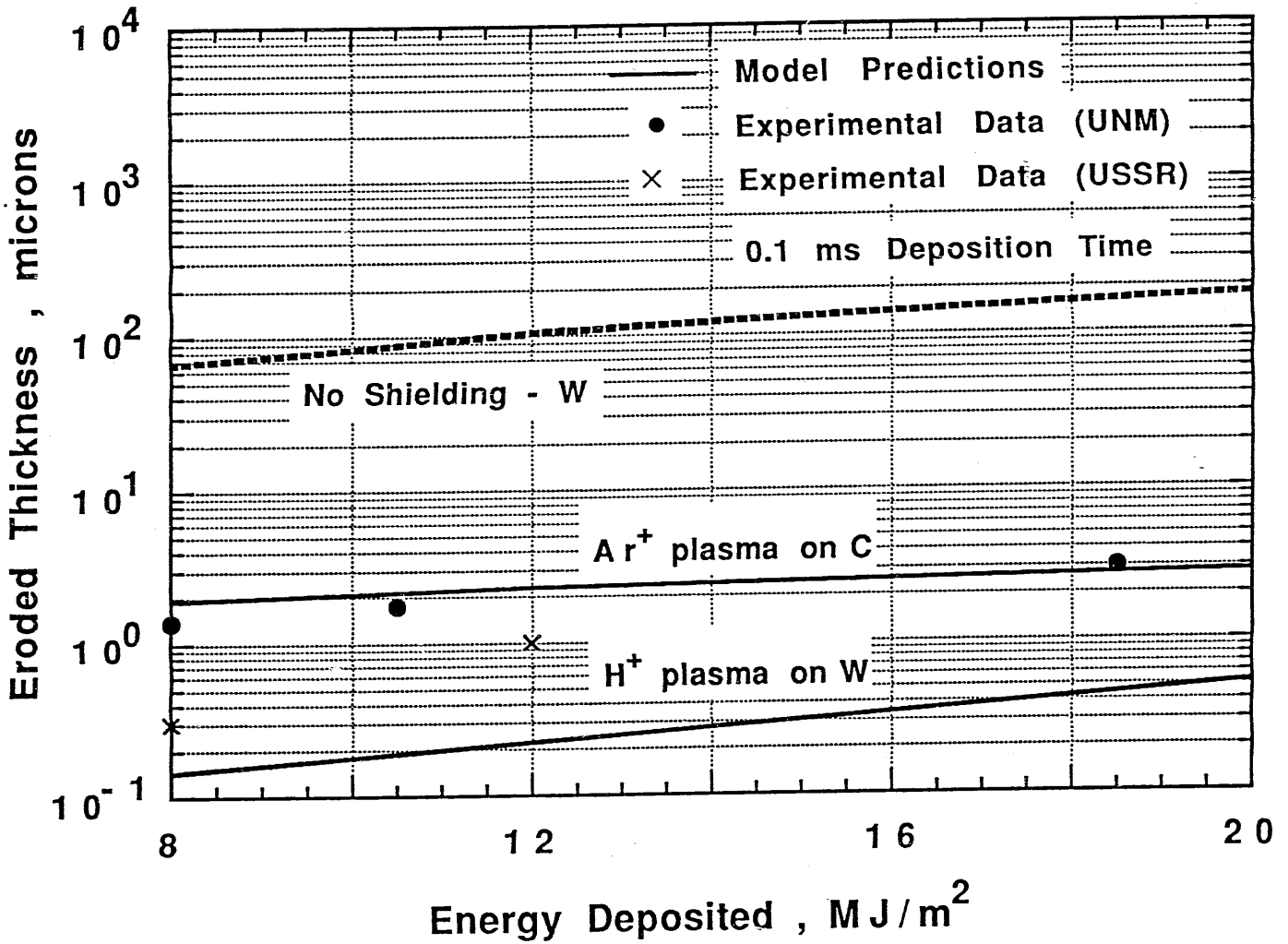
Model Predictions
Experimental Data (UNM)
Experimental Data (USSR)
0.1 ms Deposition Time
No Shielding - W
Ar+ plasma on C
H+ plasma on W
Eroded Thickness , microns
Energy Deposited , MJ/m2
10^4
10^3
10^2
10^1
10^0
10^-1
8
12
16
20

FIGURE 8

DATE
FILMED
8107192